Sensors and Materials, Vol. 32, No. 7 (2020) 2321–2328
MYU Tokyo

S & M 2261

Photoelectric Properties of SnO_2/Ti/GZO Multilayer Thin Film after Annealing at Different Temperatures for Photosensor Applications

Chi-Fan Liu, Tao-Hsing Chen,* and Yu-Sheng Huang

Department of Mechanical Engineering, National Kaohsiung University of Science and Technology, Kaohsiung 807, Taiwan

(Received February 11, 2020; accepted May 25, 2020)

Keywords: SnO_2, multilayer film, annealing temperature, electrical, transmittance

In this study, RF magnetron sputtering is employed to deposit a SnO_2/Ti/GZO (TTG) transparent conductive film on a Corning glass substrate to investigate the effect of the annealing temperature on the electrical properties, transmittance characteristics, surface properties, and structural properties of a TTG conductive film. The results show that upon annealing at 300 ℃, the minimum resistance was achieved by the TTG multilayer film, i.e., 1.57×10^{-2} Ω·cm. Regarding the transmittance characteristics of all multilayer films, it is evident that the higher the annealing temperature, the higher the mean transmittance, but above an annealing temperature of 300 ℃, the transmittance decreases slightly.

1. Introduction

In the visible light and near-IR regions, a transparent conductive oxide (TCO) can exhibit excellent conductivity and high optical transmittance. Owing to these characteristics, TCO films can be widely applied in a variety of photoelectric components such as solar cells,[1,2] organic light-emitting appliances,[3,4] thin-film transistors,[5,6] photovoltaic batteries,[7–9] electrochromic devices,[10] and tablet displays.[11–14] Normally, metallic films are opaque to visible light. When the thickness of a metallic film is below 100 Å, it allows visible light to be transmitted while exhibiting greater reflectivity in the IR region. Materials with energy gaps larger than 3 eV should be used to form semiconductors, for example, In_2O_3, ZnO, SnO_2, TiO_2, and CdO,[15] which can be used as semiconductor materials.

Research to achieve better conductivity and transmittance has been conducted in recent years.[16–18] It has been proposed that oxide and metallic films can be stacked together to form a three-layer transparent conductive film of the form oxide/metal/oxide or metallic oxide/metal/metallic oxide,[19] which is called a sandwiched film or multilayer film. Such films can not only prohibit the reflection of visible light by the metallic layer but can also transmit visible light.[20–23]

*Corresponding author: e-mail: thchen@nkust.edu.tw
https://doi.org/10.18494/SAM.2020.2867

ISSN 0914-4935

In industry, SnO_2 was commercialized earlier than Ga-doped ZnO (GZO). Despite the inferior electrical properties of SnO_2 to those of GZO, its photoelectric properties are superior to those of GZO in the IR region above a wavelength of 600 nm. In addition to having high chemical stability and heat stability, SnO_2 can also be used to configure the tissue structure on a film surface to enlarge the working wavelength range. Because of these characteristics, SnO_2 conductive films are now widely applied in gas sensors or as the electrodes of solar energy batteries; therefore, they are extensively used in modern buildings. Transparent conductive SnO_2 films have also been widely used in low-radiation glass. However, it is still extremely difficult to apply these films in tablet displays owing to their high resistance and poor resistance to erosion.

In this research, Ti element is selected to constitute the intermediate metallic layer when using RF magnetron sputtering to deposit a SnO_2 sandwiched multilayer film. Ti is selected because its maximum chemical valence is +4.[24] The radius of Ti^{4+} is 0.0605 nm and that of Sn^{4+} is 0.069 nm. Because of the similar radii, Ti^{4+} can replace Sn^{4+} at the same position in the crystal lattice of SnO_2. As such, the interface between the Ti layer and the SnO_2 layer will not exhibit significant lattice twisting, thus reducing the scattering of light in the interface between the two layers. Finally, SnO_2/Ti/GZO (TTG) films are annealed in order to find a sandwiched multilayer film that can exhibit optimal electrical and optical properties.[25]

2. Experimental Methodology

In the experimental process, a Corning glass substrate was used. To begin with, the glass substrate was cut into pieces of the same size [i.e., 25 mm (length) × 25 mm (width) × 7 mm (thickness)]. Next, the glass substrates were cleaned sequentially in deionized (DI) water, acetone, isopropanol, then DI water again to wash off the non-organic compounds. Finally, the DI water was used to remove the residual solvent and then the specimens were loaded into a 90 ℃ oven until the water was completely vaporized. An RF sputtering system was employed for film deposition, and the sputtering was then executed after adjusting the required process parameters. During the sputtering process, we did not heat the substrate or charge additional gas. The purpose of this experiment was to study the impact of different annealing temperatures on the characteristics of transparent conductive films. The films were also annealed and the properties of the films were analyzed before annealing and after annealing at 200, 300, 400, and 500 ℃. We used X-ray diffraction (XRD) to investigate the crystal growth of these multilayer thin films. We used a TENCOR (Alpha-Step 500) surface profilometer to measure the thickness of the films, scanning electron microscopy (SEM) to analyze the surface features, and atomic force microscopy (AFM) to investigate the roughness and grain size.

3. Results and Discussion

After the multilayer film was deposited by sputtering at a low power, annealing was conducted in a vacuum environment for 20 min at 200, 300, 400, or 500 ℃.

3.1 Thickness comparison

As shown in Table 1, the vacuum annealing temperature slightly affected the thickness of the TTG three-layer film. This means that the total thickness of the multilayer film was maintained regardless of the annealing temperature.

3.2 Comparison of XRD properties after annealing of TTG multilayer film

Figure 1 shows the structural properties of the TTG multilayer films obtained by XRD. Peaks appear in the spectra of the TTG multilayer films annealed at 300 to 500 °C at angles of 26.6, 34.5, and 51.7°. These values correspond to (110), (002), and (211) phases, respectively. The (002) phase corresponds to ZnO. This suggests that Sn or Ti atoms can be replaced by a diffusion process following the annealing process.[26,27] The ZnO peak intensity was lowest after annealing at 300 °C. This means that the crystallized phase $SnO{\cdot}SnO_2(Sn_2O_3)$ existed inside the structure of the TTG multilayer film. After annealing at 400 and 500 °C, the $SnO{\cdot}SnO_2(Sn_2O_3)$ peak was observed at 26.6°, which corresponds to the (110) phase. As such, the Sn_2O_3 phase will affect the subsequent electrical properties.

3.3 Analysis of electrical properties

The annealing was performed after the sputtering deposition of the TTG multilayer film. Table 2 shows the change in the electrical properties of the films with the annealing

Table 1
Thickness of TTG after annealing at different temperatures.

TTG	
Annealing temperature (°C)	Thickness (nm)
as-deposited	176.729
200	176.929
300	178.98
400	178.7
500	181.25

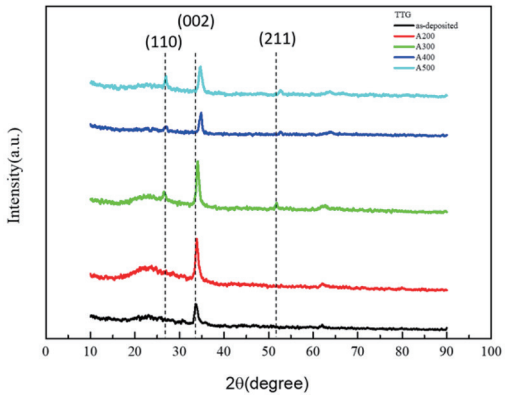

Fig. 1. (Color online) XRD spectra of TTG annealed at different temperatures.

Table 2
Electrical properties of TTG after annealing at different temperatures.

TTG: SnO_2 50 W 20 min / Ti 40 W 5 min / GZO 100 W 20 min			
Annealing temperature (°C)	Resistivity (Ω·cm)	Mobility (cm^2/Vs)	Carrier concentration (cm^{-3})
as-deposited	2.73×10^{-2}	2.24	1.04×10^{20}
200	1.73×10^{-2}	2.32	1.7×10^{20}
300	1.57×10^{-2}	4.55	2.1×10^{20}
400	6.19×10^{-2}	12.9	1.11×10^{19}
500	4.82×10^{-2}	12.8	1.02×10^{19}

temperature. The resistivity was a minimum of 1.57×10^{-2} Ω·cm after annealing at 300 °C, which was mainly due to the highest carrier concentration. The resistivity was higher after annealing at a higher temperature. The main reason for this was probably the doping of Sn^{4+} ions, which formed a Sn_2O_3 phase with higher resistivity, as indicated by the XRD data.

3.4 Transmittance of TTG multilayer film

From Tables 3 and 4 and Figs. 2 and 3, we can see the transmittance properties of the TTG multilayer films. Before annealing, the mean transmittance of the TTG multilayer film was 63.85%, and the low transmittance was mainly caused by the reflection from the mirror effect of the intermediate Ti layer. The transmittance properties significantly improved with increasing annealing temperature. The optical energy gap of a conventional GZO film tends to increase as soon as the carrier concentration increases. This is mainly because the Fermi level moves into the conduction band and the electrons on the valence band are forced to jump to the conduction band, thereby requiring more energy, and the so-called Burstein–Moss effect is therefore induced.[28] However, the opposite phenomenon was seen during the experimental process, where the optical energy gap increased with decreasing carrier concentration. This phenomenon could be due to the interaction between ionic compounds. For example, Zn^{2+} and Sn^{4+} ions coexisted in the GZO films, which may have generated donor–acceptor pairs, thus

Table 3
Comparison of optical properties of TTG after annealing at different temperatures.

Transmittance average (%)	
Annealing temperature (°C)	TTG
as-deposited	63.85
200	69.34
300	90.14
400	87.15
500	87.79

Table 4
Comparison of energy gap of TTG after annealing at different temperatures.

Energy gap (eV)	
Annealing temperature (°C)	TTG
as-deposited	2.95
200	3.1
300	3.21
400	3.15
500	3.17

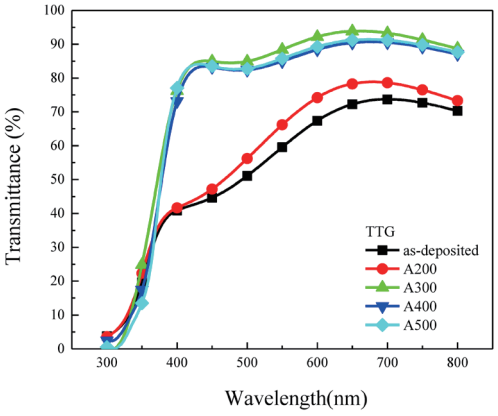

Fig. 2. (Color online) Transmittance of TTG after annealing at different temperatures.

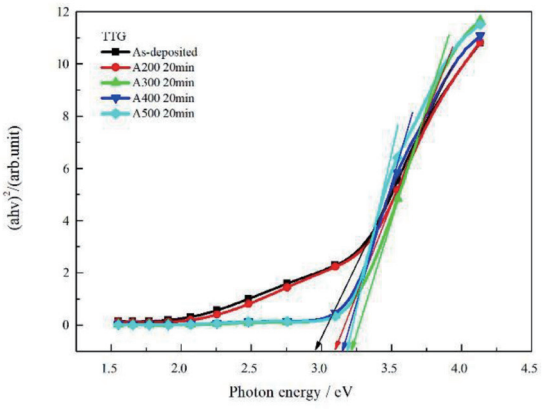

Fig. 3. (Color online) Energy gap of TTG after annealing at different temperatures.

shrinking the energy gap and offsetting the Burstein–Moss effect.[29] Although the carrier concentration decreased with increasing annealing temperature, the energy gap and the mean transmittance increased. In particular, after annealing at 200 ℃, the crystallinity of the thin film was increased and the mean optical transmittance was increased to about 70%. The TTG film annealed at 300 ℃ was crystalline and its optical transmittance reached nearly 90%. The large increase in the transmittance should be due to the lattice disorder or surface-interface-related defects found in the crystalline film.[29]

3.5 Surface feature analysis

From Table 5 and Figs. 4 and 5, we can see the impact of the increased annealing temperature of the TTG multilayer film on the surface topography and the distribution of crystal grains. The surface roughness Ra before and after annealing has an average value of about 0.2–0.4. After annealing at 300 ℃, *Ra* remains at about 0.375 nm. The crystal grains started to crystallize from 300 ℃ and the surface formed a crystallized pattern and *Ra* therefore increased. From SEM and AFM images, we can see that the TTG multilayer film has a flatter surface before the annealing and when subjected to annealing at 200 ℃. After annealing at 300 ℃, the surface forms a phase–island valley structure with higher roughness due to greater fluctuation.

Table 5
Roughness of TTG annealed at different temperatures.

Annealing temperature (℃)	*Ra* (nm)
as-deposited	0.253
200	0.308
300	0.375
400	0.350
500	0.345

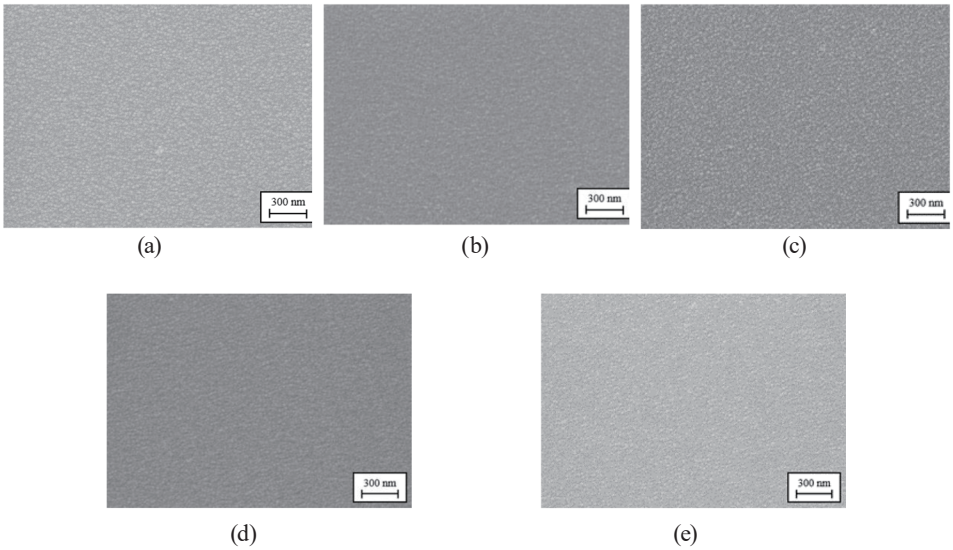

Fig. 4. SEM images of TTG annealed at different temperatures: (a) as-deposited, (b) annealed at 200 ℃, (c) annealed at 300 ℃, (d) annealed at 400 ℃, and (e) annealed at 500 ℃.

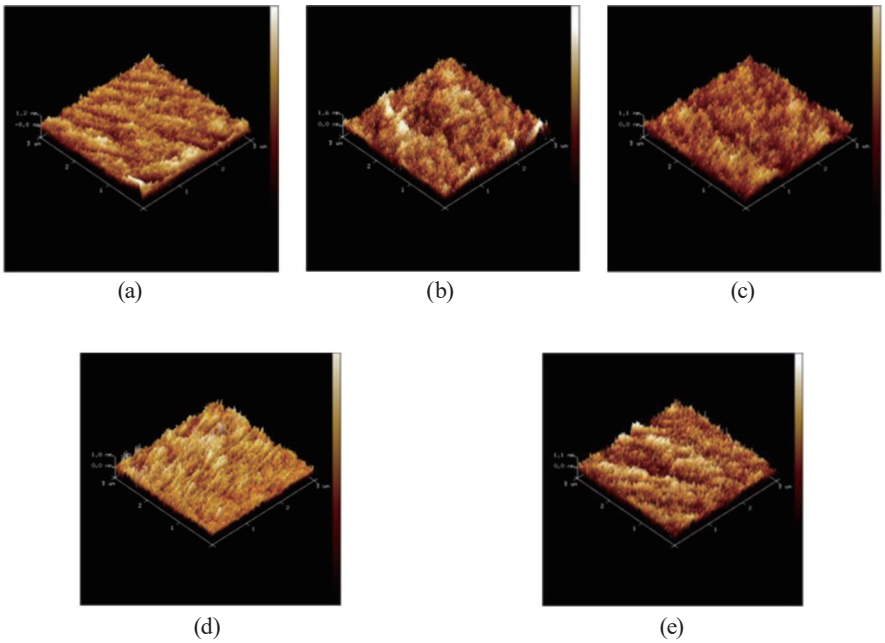

Fig. 5. (Color online) AFM images of TTG annealed at different temperatures: (a) as-deposited, (b) annealed at 200 °C, (c) annealed at 300 °C, (d) annealed at 400 °C, and (e) annealed at 500 °C.

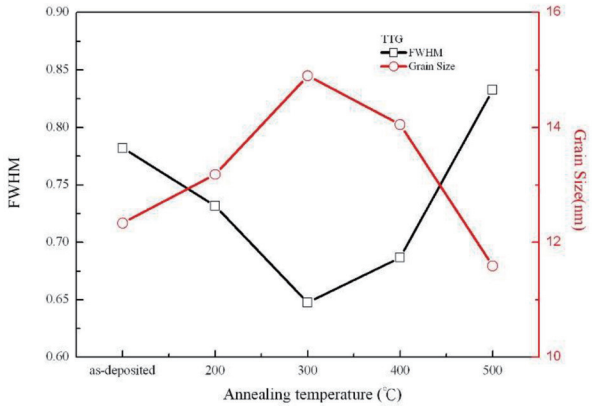

Fig. 6. (Color online) Grain size of TTG multilayer films annealed at different temperatures.

3.6 Analysis of grain size

From the XRD peak value, the full width at half maximum (FWHM) can be calculated using Scherrer's formula[30] as

$$D = 0.9\lambda/\beta\cos\theta, \tag{1}$$

where D is the grain size, β is the XRD peak FWHM, λ is the wavelength of the incident X-ray, and $\cos\theta$ is the diffraction angle of incident light. λ and $\cos\theta$ are constant values, so β becomes the most important factor, as shown in Fig. 6. Because λ and θ are fixed values and D and β

have a reciprocal relation, the smaller the FWHM, the larger the crystal grains.[29] The crystal grain size increases with the annealing temperature up to 300 ℃ but then decreases. When the annealing temperature is 300 ℃, the crystal grain size has a maximum value of 14.9 nm.

4. Conclusions

The experimental results indicated that the thickness of the TTG multilayer film is not affected by the annealing temperature. According to the results of XRD structure analysis, the TTG multilayer film has (110), (002), and (211) phases. Furthermore, the TTG multilayer film has a minimum resistance of 1.57×10^{-2} Ω·cm after annealing at 300 ℃. The TTG multilayer film has a maximum mean transmittance of 90.14% after annealing at 300 ℃, and the energy gap is 3.21 eV. According to surface feature observation, the *Ra* value increased with increasing annealing temperature up to 300 °C, above which it decreased. The crystal grain size also increased with increasing annealing temperature up to 300 °C and then decreased. Our experimental results show that TTG multilayer thin films can be used as a TCO and as the photoabsorbing layer in photosensors. Furthermore, they can inhibit the transmission of light of some wavelengths in photosensors.

Acknowledgments

The authors would like to express their sincere gratitude to the Ministry of Science and Technology, Taiwan, which sponsored the work under Contract No. 106-2628-E-992-302-MY3.

References

1 K. Fleischer, E. Arca, and I. V. Shvets: Sol. Energy Mater. Sol. Cells **101** (2012) 262.
2 W. Sun, S. Wang, S. Li, X. Miao, Y. Zhu, C. Du, R. Ma, and C. Wang: Solar Cells. Coatings **9** (2019) 320.
3 M. Oh and I. Seo: J. Electron. Mater. **43** (2014) 1232.
4 N. Najaf and S. M. Rozati: Acta Phys. Pol. A **131** (2017) 222.
5 B. Jang, T. Kim, S. Lee, W. Y. Lee, H. Kang, C. S. Cho, and J. Jang : IEEE Electron Device Lett. **39** (2018) 1179.
6 R. E. Presley, C. L. Munsee, C. H. Park, D. Hong, J. F. Wager, and D. A. Keszler: J. Phys. D: Appl. Phys. **37** (2004) 2810
7 C. Kim, M. Noh, M. Choi, J. Cho, and B. Park: Chem. Mater. **17** (2005) 3297.
8 R. Riveros, E. Romero, and G. Gordillo: Braz. J. Phys. **36** (2006) 1042.
9 A. J. Haider, A. J. Mohammed, S. S. Shaker, K. Z. Yahya, and M. J. Haider: Energy Procedia **119** (2017) 473.
10 P. S. Patil, S. B. Sadale, S. H. Mujawar, P. S. Shinde, and P. S. Chigare: Appl. Sur. Sci. **253** (2007) 8560.
11 T. Isono, T. Fukuda, K. Nakagawa, R. Usui, R. Satoh, E. Morinaga, and Y. Mihara: J. Soc. Inf. Disp. **15** (2007) 161.
12 P. Patel, A. Karmakar, C. Jariwal, and J. P. Ruparelia: Procedia Eng. **51** (2013) 473.
13 A. J. Haider, S. S. Shaker, and A. H. Mohammed: Energy Procedia **36** (2013) 776.
14 S. H. Lee, K. Kwon, K. Kim, J. S. Yoon, D. S. Choi, Y. Yoo, C. Kim, S. Kang, and J. H. Kim: Materials **12** (2019) 137.
15 E. Shanthi, A. Banerjee, V. Dutta, and K. L. Chopra: J. Appl. Phys. **53** (1982) 1615.
16 T. H. Chen and T. Y. Chen: Nanomaterials **5** (2015) 1831.
17 T. H. Chen and B. L. Jiang: Opt. Quant. Electron **48** (2016) 77.
18 T. H. Chen, C. C. Chiang, and T. Y. Chen: Microsyst. Technol. **32** (2017) 1687.
19 T. H. Chen and H. T. Su: Sens. Mater. **30** (2018) 2541.

20 J. C. C. Fan, F. J. Bachner, G. H. Foley, and P. M. Zavracky: Appl. Phys. Lett. **25** (1974) 693.
21 K. A. Zahidah, S. Kakooei, M. C. Ismail, H. Mohebbi, M. Kermanioryani, and P. B. Raja: Int. J. Eng. Technol. Innov. **7** (2017) 243.
22 F. H. Wang, C. S. Wang, and H. W. Liu: Proc. Eng. Technol. Innov. **13** (2019) 26.
23 R. W. You and Y. P. Fu: Adv. Technol. Innov. **2** (2016) 95
24 W. S. Liu, W. T. Hsieh, S. Y. Chen, and C. S. Huang: Solar Energy **174** (2018) 83.
25 M. W. Wang, T. H. Chen, H. D. Su, and Y. S. Huang: Microsyst. Technol. (2019) (in press).
26 M. G. Sousa and A. F. da Cunha: Appl. Sur. Sci. **484** (2019) 257.
27 S. Song, T. Yang, J. Liu, Y. Xin, Y. Li, and S. Han: Appl. Sur. Sci. **257** (2011) 7061.
28 Y. Wang and W. Tang: Solid-State Electron. **138** (2017) 79.
29 B. D. Cullity and S. R. Stock: Elements of X-ray diffraction (Prentice Hall, 2001) Chap. 5-2, pp. 167–171.
30 M. Caglar, S. Ilican, and Y. Caglar: Thin Solid Films **517** (2009) 5023.

About the Authors

Chi-Fan Liu received his M.D. degree from the University of the Incarnate Word, U.S.A., in 2002. Since 2004, he has been an associate professor at Feng Chia University, Taiwan. Since 2019, he has been Head of Yuchi Township, Nantou County, Taiwan. Now, he is a Ph.D. graduate student at the National Kaohsiung University of Science and Technology, Department of Mechanical Engineering, Kaohsiung, Taiwan. His research interests are in thin films, sport science, bioengineering, and sensors.

Tao-Hsing Chen received his B.S. degree from National Cheng Kung University, Taiwan, in 1999 and his M.S. and Ph.D. degrees from the Department of Mechanical Engineering, National Cheng Kung University, in 2001 and 2008, respectively. From August 2008 to July 2010, he was a postdoctoral researcher at the Center for Micro/Nano Science and Technology, National Cheng Kung University. In August 2010, he became an assistant professor at National Kaohsiung University of Applied Sciences (renamed National Kaohsiung University of Science and Technology), Taiwan. Since 2016, he has been a professor at National Kaohsiung University of Science and Technology. His research interests are in metal materials, TCO thin films, thermal sensors, and photosensors. (thchen@nkust.edu.tw).

Yu-Sheng Huang received his B.S. degree from I-Shou University, Taiwan, and his M.S. degree from National Kaohsiung University of Science and Technology in 2019. He is now serving in the military.